Journal of Experimental Botany, Vol. 73, No. 5 pp. 1385–1401, 2022
https://doi.org/10.1093/jxb/erab469 Advance Access Publication 27 October 2021

RESEARCH PAPER

Quantification of the pluriannual dynamics of grapevine growth responses to nitrogen supply using a Bayesian approach

Sylvain Vrignon-Brenas[1], Bénédicte Fontez[2], Anne Bisson[2,3], Gaelle Rolland[1], Jérôme Chopard[3], Damien Fumey[3], Aurélie Metay[4], and Anne Pellegrino[1,*]

[1] LEPSE, Univ Montpellier, INRAE, Institut Agro, 2 Place Pierre Viala, 34060 Montpellier, France
[2] MISTEA, Univ Montpellier, INRAE, Institut Agro, 2 Place Pierre Viala, 34060 Montpellier, France
[3] itk, Cap Alpha, Avenue de l'Europe, 34830 Clapiers, France
[4] ABSys, Univ Montpellier, CIRAD, INRAE, Institut Agro, 2 Place Pierre Viala, 34060 Montpellier, France

* Correspondence: anne.pellegrino@supagro.fr

Received 31 March 2021; Editorial decision 19 October 2021; Accepted 26 October 2021

Editor: Yves Gibon, INRAE-Bordeaux, France

Abstract

The effect of nitrogen (N) nutrition on grapevine carbon (C) dynamics has been well studied at the annual scale, but poorly addressed at a pluriannual timescale. The aim of this study was to quantify, in an integrated conceptual framework, the effect of N nutrition on potted grapevine growth and storage over 2 consecutive years. The consequences of using destructive measurements were investigated using a hierarchical Bayesian model. The rate and duration of leaf growth were both positively impacted by the chlorophyll content of the leaves, but they were negatively impacted by the initial carbohydrate measurements, raising a distortion in the estimation of initial reserves. The C production per unit of global radiation depended on the leaf area dynamics. The allocation of dry matter mainly relied on the phenological stage. The present study highlights the importance of using appropriate statistical methods to overcome uncertainties due to destructive measurements. The genericity of the statistical approach presented may encourage its implementation in other agronomy studies. Based on our results, a simple conceptual framework of grapevine pluriannual growth under various N supplies was built. This provides a relevant basis for a future model of C and N balance and responses to N fertilization in grapevine.

Keywords: Carbon, grapevine, growth, hierarchical Bayesian model, nitrogen, storage.

Introduction

Nitrogen (N) is a critical limiting element in agricultural systems. Numerous studies on annual and perennial species have shown that low N inputs can negatively impact yield development and fruit metabolism, thus altering the production in terms of both quantity and quality (Ekbic *et al.*, 2010; Brunetto *et al.*, 2015). The effect of N status on grapevine carbon (C) growth and storage has been well studied at the annual scale, but only poorly addressed at the pluriannual timescale due to

Abbreviations: C, carbon; DM, dry matter; N, nitrogen; TNC, total non-structural carbohydrates.

difficulties such as controlling N cycling and availability in the field, quantifying C and N storage in roots, and convincing winemakers to sacrifice grapevines and their associated yield for destructive measurements to be made on them. In this context, potted grapevine experiments appear to be a satisfactory alternative to study C and N allocation at the pluriannual scale in semi-controlled conditions.

The seasonal dynamics of C and N assimilation and storage share consistent patterns. Grapevines, like other woody plants, are particularly reliant on C and N reserves to support growth (Loescher *et al.*, 1990; Mooney and Gartner, 1991). From budburst to flowering, the reserves in woody tissues progressively decrease to reach a minimum around flowering (Yang and Hori, 1980; Conradie, 1991; Bates *et al.*, 2002; Zapata *et al.*, 2004; Holzapfel *et al.*, 2010). Low N or C storage can affect early vegetative growth, reducing leaf area (Metay *et al.*, 2014; Vrignon-Brenas *et al.*, 2019). Low N supply also reduces C production over the season through its negative effect on leaf net photosynthesis, as has been reported for a wide range of species, including grapevine (Evans, 1989; Prieto *et al.*, 2012). Ultimately, a low C pool resulting from low reserves and/or photosynthetic activity can negatively affect all phases of reproductive development (from the initiation of inflorescences in latent buds to individual berry growth) and reduce the final yield (Keller, 2010). The reallocation of C and N to the woody tissues occurs once root N uptake or reallocation from leaves and photosynthetic activity exceeds berry demand, generally after the plateau of berry sugar loading (Zapata *et al.*, 2004; Pradubsuk and Davenport, 2010; Rossouw, 2017).

The allocation of biomass towards the annual and perennial organs is critical for both the productivity and the sustainability of perennial crops. Yet, the C:N ratio has been shown to impact the rules of biomass allocation among organs. For instance, N deprivation enhanced root growth at the expense of aboveground growth in grapevine (Grechi *et al.*, 2007). To date, the optimization of N supply is hampered by the lack of an unequivocal theory for explaining the underlying mechanisms of grapevine dry matter (DM) distribution among organs at the pluriannual timescale. As a result, most of the existing grapevine models simulate the C balance in vines under abiotic constraints at a seasonal timescale (Lakso and Poni, 2005), and only a few models integrate the pluriannual C dynamics (Bindi *et al.*, 1997) or the N constraints (Nendel and Kersebaum, 2004; Garcia de Cortazar-Atauri, 2006), or both (Nogueira Júnior *et al.*, 2018). Vrignon-Brenas *et al.* (2019) investigated, as a first step, the hierarchical responses of grapevine C functioning to N supply over two successive seasons. However, this study underlined the need to implement specific statistical methods appropriate to the structure of the dataset. Indeed, explanatory variables (nutritional status) and dependent variables (development, growth) involve different plant samples due to the destructive nature of the measurement of explanatory variables. As a result, the independent variables, also known in a statistical context as regressors, are measured with errors. The estimation based on the standard assumption leads to inconsistent estimates, meaning that the parameter estimates do not tend to true values even in very large samples. For simple linear regression the effect is an underestimation of the coefficient, known as the attenuation bias (Chesher, 1991). As such, those models account only for errors in the dependent variable (Draper and Smith, 1998). Ultimately, improving the experimental design cannot solve this issue, and there is a need to use appropriate statistical methods. Interesting questions from a statistics-based methodological viewpoint are raised by such experimental designs making use of destructive measurements. As underlined by Jensen *et al.* (2020), there has been an increased awareness of the use of appropriate statistical methods in agronomy. Measurement error often occurs in field designs because some covariates, due to destructive measurements, have been measured on different individuals rather than variables of interest, and with a different frequency, inducing an 'in and out of the sample' error. Another fundamental issue in agronomy is the complexity of the biological processes, which often imply simultaneity or composite variables. Indeed, the Bayesian approach appears relevant to account for covariates with measurement error and composite variables. Thus, the need to account for measurement error arises in different topics in agronomy, for example, to evaluate unbiased productivity in agriculture (Abay *et al.*, 2019), or to develop sensors and spatialized data (Pollice *et al.*, 2019). Moreover, the hierarchical Bayesian modelling approach as a natural route for accommodating measurement error uncertainty in regression models is advocated for in the literature for both theoretical and real cases (Arima *et al.*, 2012; Muff *et al.*, 2015; Pollice *et al.*, 2019). Ultimately, the flexibility of the Bayesian framework allows the integration in one unique model of all the simultaneous equation sub-models, the measurement errors (hierarchical sub-models), and latent (or composite) variables. The Markov chain Monte Carlo (MCMC) method enables a numerically efficient implementation and estimation of this kind of integrated hierarchical model.

The aim of this study was to quantify, based on an integrated conceptual framework, the pluriannual effect of N supply on grapevine growth and development processes by integrating the temporal dynamics over the years. To do so, we assume that (i) C production per unit of incident global radiation is piloted by the leaf area, this latter depending on SPAD meter (SPAD-502, Konica-Minolta, Osaka, Japan) measurements and C reserves, and (ii) the Bayesian approach is relevant to account for covariates with measurement error and composite variables, and therefore to analyse destructive measurements. Five experiments conducted on three batches of potted Sauvignon blanc grapevines over 3 years from 2017 to 2019 were used to quantify the relationships between N supply, leaf area, and DM dynamics.

Materials and methods

Plant material and growth conditions

Five experiments (hereafter called Exp.1.1, Exp.1.2, Exp.2.1, Exp.2.2, and Exp.3.1) were conducted on three batches (or plant lots) of potted Sauvignon blanc grafted on to SO4 rootstock over 3 years from 2017 to 2019 (Table 1), which represented a global population of 110–150 plants. The experiments were named as the combination of the batch (1–3) and experimental year (1 or 2). Plants were grown outside at the Montpellier-SupAgro Campus (43′83″N, 38′53″E) in the south of France. They were 2–3 year-old during the first and second successive years of the experiments for batches 1 and 2, and 2-year-old during the single year of the experiment for batch 3.

The roots of the plants in batches 1 and 2 were severely pruned before planting (on 19 April 2017 for batch 1 and 7 March 2018 for batch 2), by cutting all the fine roots. Then, the pots (10 litres) were filled with a mixture of frozen black sphagnum peat moss, peat fibre, fine clay, and blond sphagnum peat moss (Klasmann, Substrat SP 15%). After budburst, the plants were pruned to one individual primary shoot and they were vertically trained. Crop load per shoot was restricted to two clusters in all experiments, except in Exp.1.1, in which only one cluster per shoot was retained. Plants were drip-irrigated. Four irrigations per day were supplied to avoid any water deficit, considering both plant leaf area and climatic demand. Soil water status was controlled using an automatic drip-irrigation system and was maintained at 80% of soil water-holding capacity for all treatments through daily pot weight measurements, and plant weight measurements at key phenological stages (budburst, flowering, veraison, and harvest). To avoid any mineral deficiency for elements other than N, all the pots were fertilized with a solution of macro- and micro-elements free of N, similar to the one described by Zerihun and Treeby (2002), twice a year for Exp.1.1 (on 31 May 2017 and 1 August 2017, corresponding to 255 cumulated thermal time (°Cd) and 716°Cd post budburst), three times a year for Exp.1.2 and Exp.2.1 (on 19 April 2018, 7 June 2018, and 25 June 2018, corresponding to 68, 478, and 966 °Cd post budburst), and four times a year for Exp.2.2 and Exp.3.1 (on 9 April 2019, 7 June 2019, 30 July 2019, and 12 August 2019, corresponding to 16, 396, 1206 and 1421 °Cd post budburst).

N treatments

Five N treatments, comprising four levels of mineral N supply (ammonitrate, NH_4–NO_3) with increasing and contrasting amounts of N (hereafter called 'a', 'b', 'c', and 'd') and one level of organic N supply (EO 4/3/5 + 3 GR, Frayssinet) (called 'e'), were imposed during each experiment to cover a wide range of plant N status (Table 1). The N treatments started 2 weeks after budburst and were applied up to veraison in five applications in Exp.1.1 and in six applications in all other experiments. The date and amount of fertilization were reasoned from the SPAD index measurements over the season (Table 1; see below for a description of the SPAD index measurement procedure) in order to reach and maintain a wide range of plant N contents. The total amount of N supplied from budburst to veraison varied from 0 to 8.61 g N per plant depending on the experiment. The SPAD index readings ranged, for an individual plant, from 11.8 to 41.6. SPAD index readings were used to provide a reliable, quick, and cheap estimation of the leaf N status.

Climatic conditions

Weather data (temperature, humidity, global radiation, wind speed, and rainfall) were monitored with a weather station installed within the experimental area. Data readings, collected every 12 min, were averaged and stored in a datalogger (CR1000, Campbell Scientific Ltd, Shepshed, UK).

The three years of the experimental period were characterized by contrasting climatic conditions during the growing period (Table 2). Notably, 2017 was marked by a higher average temperature from budburst to flowering (up to +3 °C) compared with 2018 and 2019. High temperatures (>35°C) were frequently observed during the period from flowering to veraison in 2019 (10 d), and from veraison to harvest in 2018 (8 d). Although the cumulated thermal time over the season in 2019 was intermediate to the ones observed in 2017 and 2018 (maximum difference of 137 °Cd), the cumulated light was the highest in 2019 (up to +640 MJ m^{-2} from budburst to harvest, compared with 2017 and 2018). Consequently, the cumulated climatic demand for water (ET0) was higher in 2019 (up to +97 mm) than in 2017 and 2018. Lastly, the pre-flowering and pre-veraison periods were particularly rainy in 2018 (up to +143 mm and +119 mm, respectively) compared with 2017 and 2019.

Plant measurements

The plant measurements performed in the experiments are listed in Table 3 and detailed in the following sections.

Phenology

The main phenological stages (budburst, flowering, and veraison) were monitored on eight plants per treatment for Exp.1.1, Exp.1.2, and Exp.2.1. For Exp.2.2, the number of plants monitored was limited (n<4) due to a heatwave period after flowering. The date of the budburst, flowering, and veraison stages corresponded to the dates at which 50% of the plants reached respectively stage 09, 61, and 81, as defined by the BBCH scale.

Table 1. Minimum and maximum N supply and SPAD index readings covering the range of all N supply treatments at three stages (flowering, veraison, and harvest) of the growing cycle period according to experiments and experimental year

Measurement	Year of measurement	Batch	Year of application of N treatments	Experiment	Flowering	Veraison	Harvest
N supply (cumulated amount from budburst) per plant (min–max) (g)	2017	1	1	Exp.1.1	0.00–0.64	0.00–2.48	
	2018	1	2	Exp.1.2	0.00–3.64	0.00–7.74	
	2018	2	1	Exp.2.1	0.00–3.64	0.00–7.74	
	2019	2	2	Exp.2.2	0.00–2.72	0.00–8.61	
	2019	3	1	Exp.3.1	0.00–2.72	0.00–8.61	
SPAD reading (min–max)	2017	1	1	Exp.1.1	28.8–33.6	19–23	17.1–28.9
	2018	1	2	Exp.1.2	19.3–38.2	17.1–35.7	19.9–34.5
	2018	2	1	Exp.2.1	25–36.5	19.5–33.3	14.8–29.8
	2019	2	2	Exp.2.2	20.6–30.6	20.4–28.1	20.2–37.9
	2019	3	1	Exp.3.1	27.2–33.9	19.4–32	15.6–29.5

Table 2. Climatic conditions over the 3 years of the experiments at different periods of the cropping season

Year	Period	Number of days	Mean temperature (°C)	Cumulated thermal time (°Cd)	Number of days with max temp >35 °C	Cumulated global radiation (MJ m^{-2})	Cumulated rainfall (mm)	Cumulated ET0 (mm)
2017	BB–FLO	35	19.1	326	0	870	43	162
	FLO–VER	49	24.8	728	3	1321	24	285
	VER–HAR	34	25.0	589	2	1277	50	254
2018	BB–FLO	50	16.6	336	0	956	195	177
	FLO–VER	57	23.6	779	1	1424	111	293
	VER–HAR	45	25.9	715	8	1509	211	299
2019	BB–FLO	61	14.4	272	0	1221	103	212
	FLO–VER	58	23.9	811	10	1546	22	323
	VER–HAR	35	25.5	550	1	1660	106	308

BB, budburst; ET0, cumulated climatic demand for water; FLO, flowering; HAR, harvest; VER, veraison.

Leaf area

The total leaf area per plant (m^2) was measured on five plants per treatment twice during the cropping season in Exp.1.2, four times in Exp.1.1, six times in Exp.2.2 and Exp.3.1, and seven times in Exp.2.1.

In Exp.1.1, Exp.1.2, and Exp.2.1, the length of each leaf was measured and converted into leaf area using the following allometric relationship, fitted during Exp.1.1 (Eq. 1):

$$\text{Leaf area} = 0.019 \times (\text{length})^2 0.492 \times (\text{length}) + 10.34 \quad (1)$$

where leaf area was expressed in cm^2 and leaf length was expressed in mm.

In Exp.2.2 and Exp.3.1, leaf area was measured using a planimeter (LI-3100C Area Meter, LI-COR Biosciences). We assumed no bias and the same error variability for the two methods of measurement (allometric relationship or planimeter).

Leaf N status

Leaf N status was assessed through measurements of chlorophyll content or SPAD index (SPAD-502, Konica-Minolta, Osaka, Japan). The SPAD index was measured on five leaves per treatment (one leaf per plant) once a week (Exp.1.1, Exp.1.2, Exp.2.1) or twice a month (Exp.2.2, Exp.3.1) from budburst up to harvest. The measurements were performed on young fully expanded leaves (10th rank from the apex) of the primary axis that were fully exposed to sunlight. Five successive readings were taken for SPAD index measurements across the whole surface of the leaf.

Non-structural carbohydrates of perennial organs

The total non-structural carbohydrates (TNC) of perennial organs (roots and wood) was measured on three plants per treatment at budburst and at harvest in all experiments, at flowering in all experiments except Exp.1.1, and at veraison in all experiments except Exp.1.1 and Exp.2.2. At budburst of the first experimental years, as no N treatment had been applied yet, six plants were sampled for each batch (i.e. in Exp.1.1, Exp.2.1, and Exp.3.1) to determine the initial TNC (common initial TNC value for all treatments).

Frozen trunk and root tissues were lyophilized for 24 h at –110 °C (Heto PowerDry LL1500, Thermo). Then, each tissue was ground to pass through a 0.1 mm mesh grid for starch biochemical measurements. A fractionation was used in which starch and other insoluble compounds in a water–ethanol mixture (20%/80%) are separated from the compounds that are soluble in this mixture, in particular sugars. In the insoluble fraction, starch was hydrolysed into glucose by autoclaving for 90 min at 110 °C followed by treatment with amyloglucosidase for 90 min at 56 °C. In the soluble fraction, which contained soluble sugars (glucose, fructose, and saccharose), a mixture of β-fructosidase, hexokinase, and phosphoglucoisomerase was used before assay by spectrophotometry at 340 nm according to the method described by Gomez *et al.* (2003) and Rolland (2020).

DM production and allocation

Between three and six plants per N treatment were sampled for destructive measurements of DM at different stages (and cumulated thermal time post-budburst; see Table 2), depending on the experiment. For Exp.1.1, plants were sampled at budburst and harvest, while for all other experiments, plants were sampled at budburst, flowering, veraison, and harvest.

Roots were carefully extracted from the soil and washed. The primary and secondary leaves, stems, clusters, trunk, and roots were separated. Trunk and root samples were frozen in liquid N and stored in the freezer (–60 °C) for analysis of the starch and soluble sugar contents (as described above). All organs were then oven-dried at 65 °C for 3–7 d and their dry weights were determined.

Table 3. Summary of the measured variables and associated statistical analyses performed depending on experiments

Variable	Measurements					Statistical approach	
	Exp.1.1	Exp.1.2	Exp.2.1	Exp.2.2	Exp.3.1	Effect of N treatments on the variable	Correlation between variables
Phenological stage (°Cd)	X	X	X	X	NA	One-way ANOVA (or Kruskal–Wallis test), Benjamini–Hochberg procedure for correction of *P*-values and Tukey HSD tests	NA
Leaf area (m^2)	X	X	X	NA	X	Piecewise regression and Bayesian hierarchical model	Bayesian error in variables model
DM accumulation (g)	X	X	X	X	X	Two-way ANOVA and one-way ANOVA at each date and Tukey HSD tests (or Kruskal–Wallis test)	Bayesian error in variables model
Carbohydrate content (g)	X	X	X	X	X		NA
Carbon allocation (%)	NA	X	X	X	X	NA	Simple linear regressions for each organ and each period

According to the conceptual framework (Fig. 1), we tested the effects of SPAD index and initial storage of the leaf area dynamics; the effects of SPAD index and leaf area on the DM accumulation; and the effect of DM accumulation on C allocation. NA, data not available.

The mean DM for each plant compartment (leaves, shoot, clusters, trunk, and roots) was determined per treatment. Then, the cumulated amount of TNC in perennial organs (roots and trunk) was subtracted from their DM to separate the 'storage' and 'perennial' DM compartments.

Lastly, the coefficients of biomass allocation towards the different organs were calculated for all experiments, except Exp.1.1, as the ratio of the gain of DM of the organ to the gain of DM of the whole plant. Four coefficients were determined over the following periods: budburst to flowering ('B1→F1' coefficient), flowering to veraison ('F1→V1' coefficient), veraison to harvest ('V1→H1' coefficient), and harvest to budburst in the following year ('H1→B2' coefficient). In our calculations, we assumed that variation of DM in a given organ and at the whole-plant level could not decrease between two stages (except for 'storage' from budburst to flowering). When this was the case, the variation of DM was considered null and the whole-plant DM was recalculated taking this correction into account.

Conceptual framework for quantifying the effects of N and C status on grapevine growth

Based on the literature, a simple conceptual framework of vine growth responses to C/N was proposed. The whole plant leaf area was related to the leaf N status and C reserves, as reported in different studies (Zufferey *et al.*, 2012, Metay *et al.*, 2014; Vrignon-Brenas *et al.*, 2019) (Fig. 1A). Then, the C production per unit of global radiation was assumed to rely on leaf area and N content (Monteith *et al.*, 1977; Prieto *et al.*, 2012) (Fig. 1B). Lastly, the responses of the biomass allocation towards each plant compartment (shoots, leaves, shoots, clusters, perennial, storage) to the total DM production per unit of global radiation were investigated (Fig. 1C).

Different statistical methods were implemented in this conceptual framework (see below and Table 3). Leaf area dynamic responses to the SPAD index (from budburst to flowering) and the initial storage

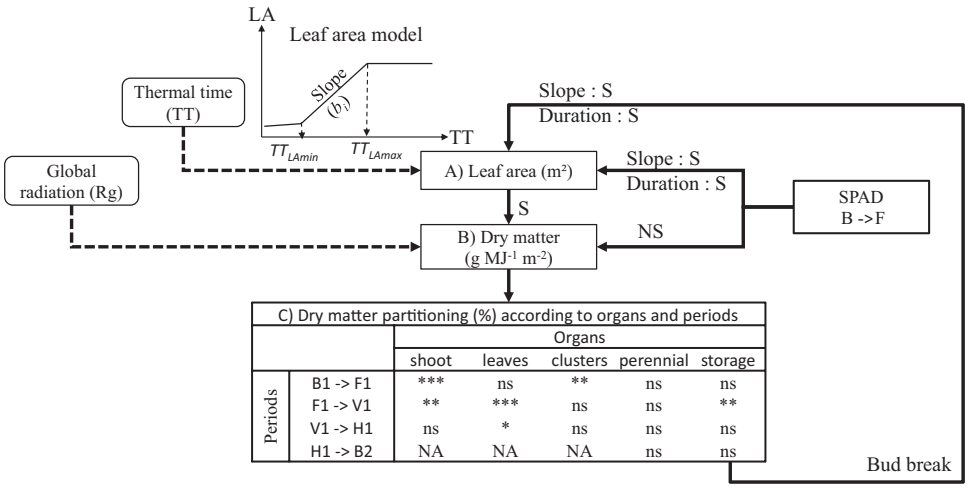

Fig. 1. Conceptual framework and quantification of the effects of SPAD index and storage on plant growth dynamics. The phenological stages are indicated using the following codes: B1, budburst the first year; F1, flowering; V1, veraison; H1, harvest; B2, budburst the second year. Bold lines represent the relationships tested and dotted lines represent intermediate variables. The effects of SPAD index and storage on the slope and duration of leaf area increase (A), and of SPAD and leaf area on DM production per unit of global radiation (B), were evaluated using a Bayesian approach. The significance of these factors (credibility of 95%) is represented as S for significant and NS for non-significant. Then, linear trends of DM production per unit of global radiation on allocation (%) were tested using *F*-tests. Asterisks represent the level of significance of the *F*-tests (**P*<0.05, ***P*<0.01, ****P*<0.001; ns, non-significant) for each organ (shoot, leaves, clusters, perennial, and storage), at each stage (B1→F1, F1→V1, V1→H1, and H1→B2). LA, leaf area; NA, data not available; TT, thermal time.

(budburst) were first fitted using a Bayesian approach. For this purpose, changes in leaf area as a function of growing degree days were fitted using piecewise linear models to calculate the slope and duration of leaf area growth for each experiment. A Bayesian approach was also used to parameterize the DM production per unit of global radiation responses to the SPAD index (from budburst to flowering) and the leaf area (at the same period as DM production). Lastly, a frequentist approach was used to address the responses of the biomass allocation towards each plant compartment over the key phenological stages to the total DM production per unit of global radiation.

Statistical analysis

All statistical analyses summarized in Table 3 and detailed hereafter were performed with the statistical program R version 3.6.2; (R Core Team, 2019).

First, we tested the phenological durations (from budburst to flowering and from flowering to veraison on all experiments, except Exp.3.1) according to the N treatment (with eight one-way ANOVA tests), adjusting for multiple ANOVA tests with Benjamini–Hochberg correction (Benjamini and Hochberg, 1995). This correction was necessary to control the rate of false significant ANOVA tests for the whole experiment.

Next, our main interest was the establishment of a conceptual framework and quantification of the effects of the SPAD index and C storage on plant growth dynamics. SPAD index measurements were not always carried out on the same individual plants as the measurements of DM and leaf area (before the use of a planimeter) because of the destructive nature of these latter measurements. The measurement of TNC was also destructive. Thus, the dataset included different samples, causing an 'in and out of the sample' error.

For the above reason, plus the hierarchical nested structure of leaf area measurements (leaf area measured at successive times on plants in a treatment and experiment), the leaf area dynamic response to SPAD index and C storage were addressed using an integrated Bayesian model. The model was based on three sub-models: (i) hierarchical piecewise linear regression of leaf area as a function of thermal time to take into account the treatment-experimentation structure, (ii) parameters of the piecewise linear regression modelled as linearly dependent of mean SPAD index and mean C storage, and (iii) random ANOVA to estimate mean SPAD index and mean C storage to deal with the measurement error due to individuals 'in and out of the sample'.

The same problem of 'in and out of the sample' led us to use a Bayesian model to assess the effect of SPAD index and leaf area on DM production, this time using two sub-models: (i) multiple linear regression and (ii) a random ANOVA to estimate mean SPAD index and deal with measurement error.

We briefly explored the relationship between plant C availability and DM allocation to complete our proposition of the conceptual framework. This part is more indicative than confirmative and should be confirmed by specific supplementary experiments. Indeed, such a method is likely to underestimate the noise and measurement errors, while increasing the risk of overestimating the number of possible effects our experimentation was really able to detect (increasing power by neglecting variability).

Effect of N on the phenological stages and associated DM accumulation

When the conditions for using parametric tests were respected [Levene's homogeneity of variances test or Shapiro–Wilk normality test not significant (P=0.05)], ANOVAs were performed to test the significance of the effect of the N treatments on (i) the duration of main phenological stages [budburst to flowering and flowering to veraison, all expressed in thermal time (TT)] and (ii) DM accumulation (at budburst, flowering, veraison, and harvest). More precisely, differences between the treatments in stage duration were tested by one-way ANOVAs (factor N treatment) for each experiment and stage (the Benjamini–Hochberg procedure was used for the correction of the P-values). Differences in DM were initially tested using two-way ANOVAs (factors N treatment and date) for each experiment. As the interactions were significant in ANOVAs (P<0.05), differences between means (N treatments) were then tested using one-way ANOVAs (factor N treatment) at each date. In all cases, significant ANOVAs (P<0.05) were followed by Tukey's HSD test to assess the differences (P<0.05) between means (N treatments). If conditions for ANOVA were not respected, non-parametric tests (Kruskal–Wallis) were performed.

Bayesian approach to account for measurement error and composite variables

Model of the leaf area dynamic response to SPAD index and storage

The dynamic of leaf area was assessed for each experiment j and N treatment i according to thermal time from budburst TT_{ij}. In order to describe this dynamic, a piecewise linear model was used over three periods: (i) a horizontal line from budburst to the onset of leaf area increase (called 'TT_{LAmin}'), (ii) a straight line from TT_{LAmin} to the thermal time when the maximum leaf area was reached (called 'TT_{LAmax}'), and (iii) a horizontal line from TT_{LAmax}, which was set at 1400 °Cd (first prior). The first transition thermal time TT_{LAmin} was set to 150 °Cd (second prior), corresponding to ~10 unfolded leaves for all conditions (experiment and treatment). In contrast, each condition (experiment and treatment) was allowed to have a different transition time to the maximum leaf area and slope, modelled/represented by a condition-specific time $TT_{\mathrm{LAmax,i}}$, and slope b_i.

Sub-model 1 Hierarchical piecewise linear regression of leaf area as a function of thermal time to take into account the treatment-experimentation structure. Let $y_{ij,i=1,\ldots,P;j=1,\ldots,N_i}$ be the leaf area value for treatment i, experiment j, and the associated TT_{ij}. Allowing for mixed trajectories, the following sub-model 1 (Eq. 2) was set:

$$y_{ij} = \mu + u(TT_{LAmax_i} - TT_{ij}) \times b_i \times (TT_{ij} - 150) + (1 - u(TT_{LAmax_i} - TT_{ij})) \times b_i \times (TT_{LAmax_i} - 150) + \varepsilon_{ij} \quad (2)$$

where ε_{ij} are assumed to be independent and normally distributed $N(0, \sigma^2)$ and a step function $u(x)$ was used such as $u(x) = 1$ *if* $x \geq 1$ and 0 to model the constraints of the horizontal lines.

Sub-model 2 Parameters of the piecewise linear regression were modelled as linearly dependent of mean SPAD index and mean storage. The slope and duration of leaf area increase $(b_i,\ TT_{LAmax_i})$ was assumed to rely on the mean SPAD index reading until flowering and the amount of mean carbohydrate reserves at budburst. This implied both composite variables and destructive measurement (for carbohydrate reserves). In this context, the integrated second sub-model 2 (Eq. 3) that included estimation of the mean explanatory variables at the same time as the estimation of the latent variables $(b_i,\ TT_{LAmax_i})$ of the leaf area dynamics was proposed:

$$b_i = \mu_b + b.slope.S \times mean(SPAD)_i + b.slope.C \times mean(storage)_i$$

$$TT_{LAmax_i} = \mu_{TT} + TT.slope.S \times mean(SPAD)_i + TT.slope.C \times mean(storage)_i \quad (3)$$

where the means are estimated at the same time with one-way random ANOVA.

Random ANOVA in a Bayesian framework A centred normal distribution for all the error terms was assumed. Variables of interest were: link with carbohydrate reserves (storage) at budburst ($b.slope.C$, $TT.slope.C$), link with SPAD index reading until flowering ($b.slope.S$, $TT.slope.S$), and individual slopes and durations (b_i, TT_{LAmax_i}).

Model of the DM production per unit of global radiation response to SPAD index and leaf area

The integrated Bayesian model to assess the effect of SPAD index and leaf area on DM production was made up of one sub-model (sub-model 3; multiple linear regression) plus the one-way random ANOVA in a Bayesian framework as described below.

Sub-model 3 The DM production per unit of global radiation responses to mean SPAD index reading values until flowering and leaf area at the same date as DM (g per plant) were fitted to the dataset. As the DM measurements were destructive, measurements were not made on the same individual plants for leaf area and DM production. The usual way to deal with this situation is to minimize the experimental variability within each condition (e.g. by the use of clones, a controlled environment, etc.) and to compute the mean values for each condition before doing a regression on mean values. Even doing this, a measurement error on the explanatory variable remains because we need to use 'out of sample' to estimate the unknown leaf area mean. The effect of this last measurement error has been studied from a theoretical and more general point of view (see Chesher, 1991). In his introduction, Chesher warns that the distortions induced by this measurement error affect statistical analysis.

Let $\gamma_{i,i=1,\ldots,p}$, be the DM production per unit of global radiation for treatment i, the following model sub-model 3 (Eq. 4) was set:

$$\gamma_i = \mu + slope.S \times SPAD_i + slope.LA \times mean(leaf\ \ area)_i + \varepsilon_i \quad (4)$$

where ε_i are assumed to be independent and normally distributed $N(0, \sigma^2)$ and the mean leaf area is estimated at the same time with one-way random ANOVA.

Random ANOVA in a Bayesian framework A centred normal distribution was assumed for all the error terms. Variables of interest were: link with leaf area ($slope.LA$) and link with SPAD index reading ($slope.S$).

Bayesian estimation and validation

Estimation In the frequentist (or classical) approach, estimation of the parameters is made by maximizing the likelihood of the vector of observations y knowing the values of the covariables (x): f(y | parameters, x). In the Bayesian approach (Gelman et al., 2004; Marin and Robert 2007, and for a review in agricultural experiments Che and Xu, 2010), parameters are random and a prior (π (parameters)) is defined by the users to represent 'model the expert knowledge'. The estimation of the parameters is done on the posterior p(parameters | y). Using the Bayes equation (under the usual condition of existence of the densities), p(parameters | y) is proportional to the product of the likelihood by the prior: f(y | parameters) × π (parameters). The posterior is a combination of data and expert knowledge. Values from the posterior distribution can be simulated via an MCMC algorithm, enabling a numerical estimation of the values of the parameters that maximize the posterior. Alternatively, to the maximum of the posterior, the posterior mean values can be used (generally when marginal posterior distributions are symmetricals).

In practice, estimation from the posterior distribution was carried out with OpenBUGS version 3.2.3 (based on BUGS, Lunn *et al.*, 2009) from R (using the R2OpenBUGS package). The estimation is based on MCMC simulation of the posterior distribution of the parameters. We ran three independent parallel chains with different starting values. The chains were run with a burn-in of 500 000 iterations. With a thinning interval of 50, the posterior mean value of the parameters was computed on 500 000 iterations. We also computed 95% credible intervals (CI) and checked the chain convergence with usual diagnostics available in the R package CODA (mainly track plots, auto and cross correlation plots, and Geweke criteria).

Validation For the leaf area dynamic model, we looked for and fitted the integrated model that best reproduced the leaf area data. We checked the marginal laws *a posteriori* for all parameters 'latent variables' (see Supplementary Fig. S1 for the histogram of the posterior distribution of the leaf area parameters).

For the DM model, the fit to the data was validated by computing the R^2 *a posteriori*. It was computed from the posterior distribution, using the formula advocated by Kvålseth (1985) (see Supplementary Fig. S1 for the histogram of the R^2 marginal posterior estimated from MCMC).

Trends of biomass allocation according to DM production

The effect of DM production per MJ on the allocation of biomass towards each compartment was estimated as described above. The trends were tested using a simple linear regression (F-test; $P<0.05$).

Results

Pluriannual effect of N supply on grapevine growth and carbohydrate storage

Whole-plant DM dynamics

The initial whole-plant DM at budburst and its evolution over the seasons widely differed between the experiments and the N treatments (Fig. 2A–C). Notably, the whole-plant DM was 2-fold higher during the first year for Exp.3.1, compared with Exp.1.1 and Exp.2.1: it was 79.6 g per plant for Exp.3.1 versus 37.2 g per plant on average for Exp.1.1 and Exp.2.1 at budburst. These differences mainly resulted from the initial root DM, as the roots were severely pruned at planting in Exp.1.1 and Exp.2.1, but not in Exp.3.1. These differences between the experiments were marked until harvest. The DM at budburst was also higher in the second year of N treatment compared with the first year, due to an increase in the root compartment (Vrignon-Brenas *et al.*, 2019). The whole-plant DM accumulation during the growing season ranged from 4.8 g to 403 g per plant depending on the experiment and the N treatment. Differences between N treatments occurred straight from budburst during year 2, although no difference was observed between N treatments before flowering in year 1. For example, the DM at budburst for Exp.2.2 varied from 67.7 g per plant for the non-fertilized treatment 'a' to 139.4 g per plant for the high-fertilized treatment 'd'. Ultimately, the highest N supply (treatments 'd' and 'c') permitted the highest DM accumulation at harvest (up to 322 g per plant),

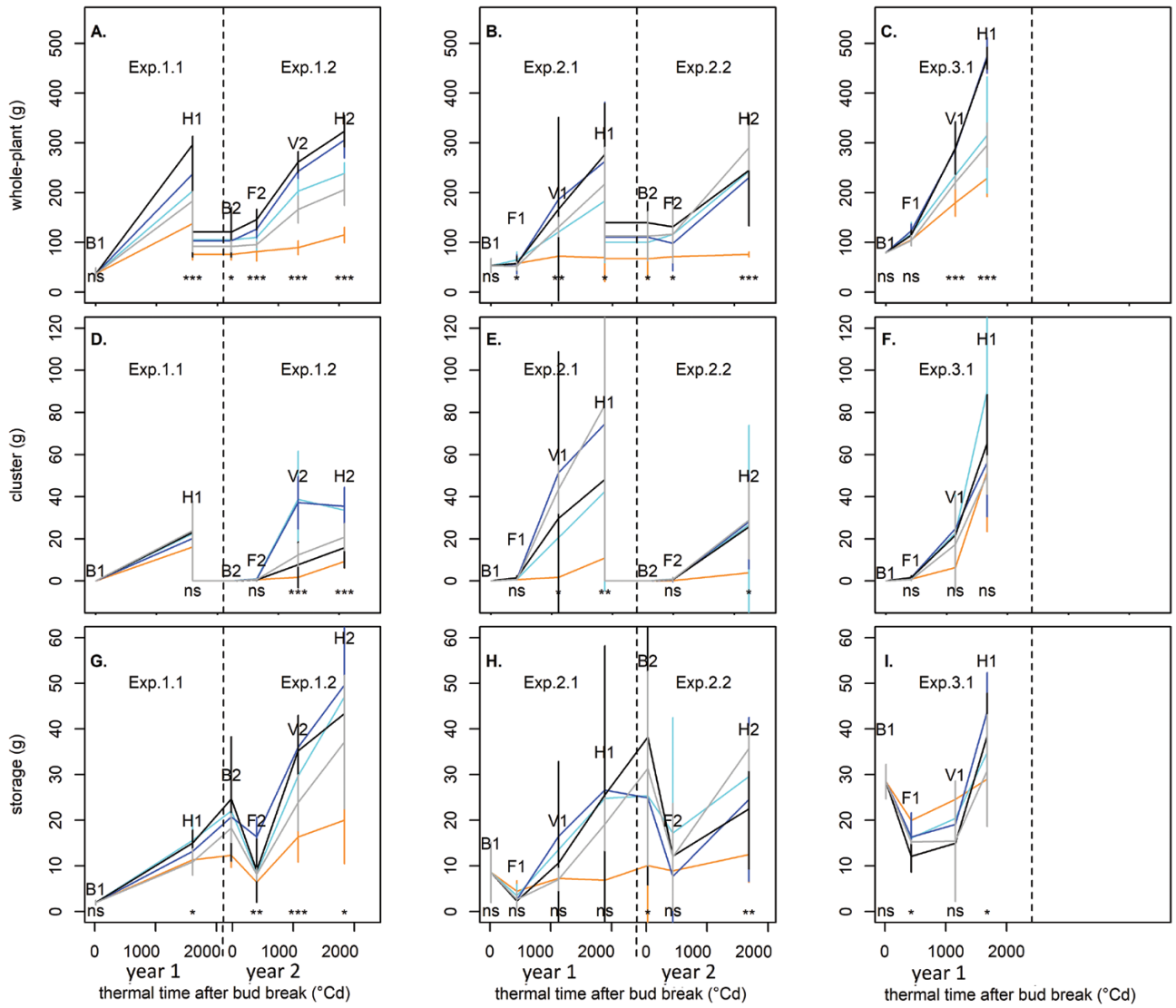

Fig. 2. Whole-plant DM, fruits (cluster) DM. and carbohydrate storage (in g per plant) as a function of cumulated thermal time after budburst (in °Cd) over the 2 successive years of N treatments for each batch (A, D, G, Exp.1.1 and Exp.1.2; B, E, F, Exp.2.1 and Exp.2.2; C, F, I, Exp.3.1; see also Table 1). The different colours represent the different N treatments (orange, a; light blue, b; blue, c; black, d; grey, e; see Materials and methods for details of the five different N treatments). Vertical lines represent the confidence intervals (α=0.05; *n*=4). The phenological stages are indicated above the curve (B1/B2, budburst in the first/second year of the experiment; F1/F2, flowering in the first/second year of the experiment; V1/V2, veraison in the first/second year of the experiment; H1/H2, harvest in the first/second year of the experiment). The effect of N at each date was tested by one-way ANOVAs or by Kruskal–Wallis test and significant differences are indicated with asterisks (**P*<0.05, ***P*<0.01, ****P*<0.001; ns, non-significant).

while the treatment which did not include N ('a') had the lowest DM accumulation (maximum of 229 g per plant for Exp.3.1 and near-zero DM accumulation in Exp.2.1 and Exp.2.2). Treatments 'b' and 'e' showed similar intermediate DM accumulations.

Cluster DM dynamics

On average (considering all experiments. and N treatments), the cluster DM represented less than 1 g per plant (2.6% of the whole-plant DM) at flowering, increased up to 22.6 g per plant (33.2% of the whole-plant DM) at veraison, and reached a maximum of 36.3 g per plant at harvest (15% of the whole-plant DM). However, the cluster DM widely differed among the experiments (Fig. 2D–F), due to the combination of several factors including the crop load (restriction to one cluster for Exp.1.1 versus two clusters for other experiments), the climatic conditions of the year, and the N treatments. For instance, cluster DM at harvest in year 1 of the experiments ranged from 16.1 g to 23.9 g per plant for batch 1 (Exp.1.1, maximum of one cluster per shoot), whereas it ranged from 10.9 g to 83.5 g per plant for batch 2 (Exp.2.1, maximum of two clusters per shoot). During the second year, the cluster DM of batch 2 (Exp.2.2, maximum of two clusters per shoot) dramatically

decreased and ranged from 3.8 g to 28.9 g per plant. Although no significant effect of N treatments was observed for Exp.1.1 and Exp.3.1 (P>0.05), the cluster DM differed among the N treatments straight from veraison for Exp.1.2 and Exp.2.1 and at harvest for Exp.2.2. For these three experiments, the cluster DM for the intermediate mineral N treatments 'b' and 'c' was significantly higher than that for the other mineral N treatments (34.4 g per plant for 'b' and 'c' versus 15.3 g per plant for 'a' and 'e', at harvest for all experiments). The organic fertilizer (treatment 'e') also permitted high cluster DM accumulation, which was ~8-fold higher at harvest (batches 1 and 2) in this treatment compared with treatment 'a' in which N was not supplied. In contrast, the equivalent mineral N treatment ('c') achieved a ~7-fold increase in the cluster DM at harvest.

Carbohydrate storage dynamics

The evolution of the pool of carbohydrates (starch, glucose, fructose, and sucrose) stored in perennial organs is shown in Fig. 2G–I. The initial storage varied among the experiments and the years. Indeed, initial storage at budburst during the first year was 2 g per plant for Exp.1.1, 8.6 g per plant for Exp.2.1, and 28.5 g per plant for Exp.3.1. During year 2, the initial storage ranged from 12.3 g per plant for the non-fertilized treatment 'a' to 20.7 g per plant on average for all other treatments. For all batches and years, carbohydrate storage sharply decreased from budburst to flowering, and then gradually increased until harvest, depending on the N treatment. The storage decrease between budburst and flowering for batch 2 was steeper during year 2 (–14.4 g per plant, Exp.2.2) than during year 1 (–5 g per plant, Exp.2.1). Differences between N treatments also tended to be more marked in the second year of the experiment. Indeed, the storage at harvest varied significantly between N treatments in the second year in Exp.1.2 and Exp.2.2 (P<0.003). Notably, storage was more than doubled when fertilization was higher in Exp.1.2 (treatments 'a' and 'c'). The same trends were observed for Exp.2.2 (treatments 'a' and 'e'), although no significant differences were observed. In contrast with other experiments, storage at flowering for Exp.3.1 was almost 2-fold higher for non-fertilized treatments ('d' and 'a'). However, similar to Exp.1.2, storage at harvest was 1.5-fold higher for the mineral N fertilized treatment 'c' compared with the unfertilized treatment 'a'.

Quantification of the effect of grapevine N status and C storage on seasonal growth

Conceptual framework for quantifying the effects of N and C status on grapevine growth

The conceptual framework presented in Fig. 1 aimed to quantify the effects of SPAD index and carbohydrate storage on the

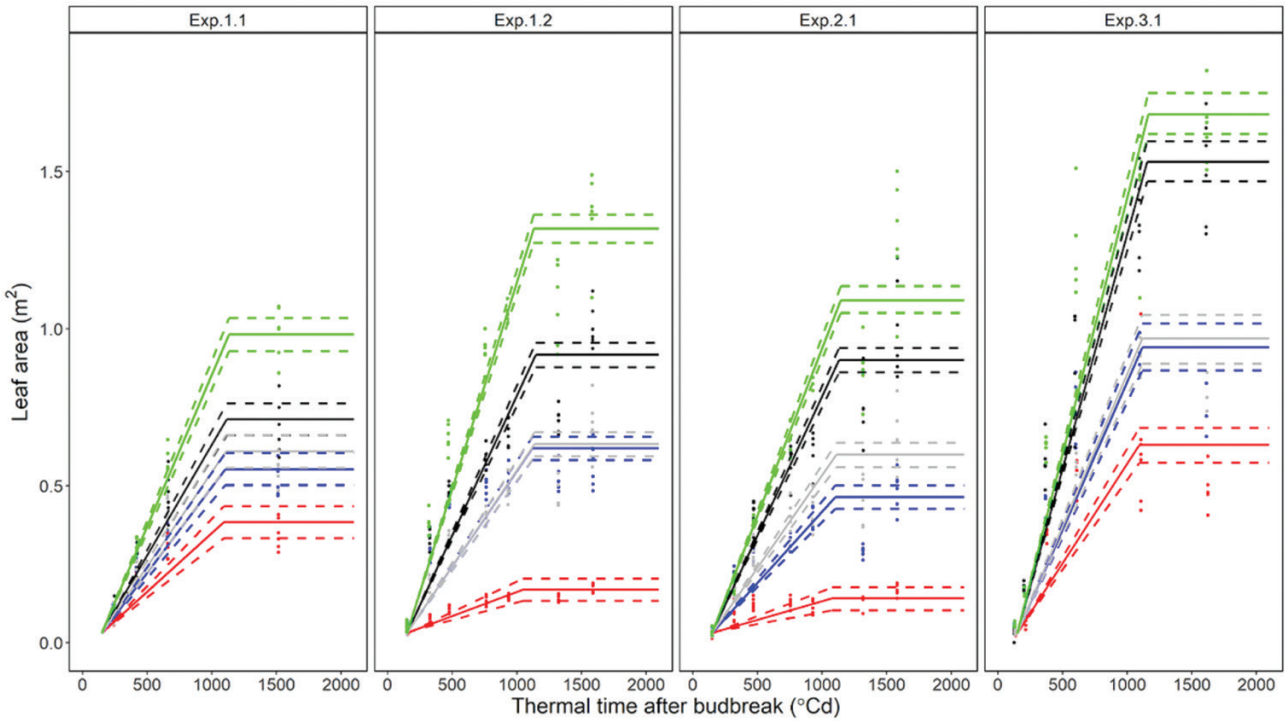

Fig. 3. Time course of leaf area (m^2) as a function of cumulated thermal time after budburst (°Cd) in the different experiments and N treatments (see Table 1). The different colours represent the N treatments (orange, a; light blue, b; blue, c; black, d; grey, e). Each point corresponds to a measurement of leaf area on an individual plant. The solid lines are the estimated leaf area dynamics for each experiment and N treatment using an integrated Bayesian piecewise linear model (see Eq. 2 and Eq. 3 for further details). The dotted lines are the upper and lower limits of the 95% credible intervals of the average estimations of leaf area.

dynamics of annual and perennial growth (see the Materials and methods for the ecophysiological assumptions). The results obtained at each step are detailed below.

Quantification of the effect of SPAD index and storage on total leaf area dynamics

The slope and duration of the whole-plant leaf area growth (respectively, b and $TT_{LASFmax}$ in Eq. 3) both decreased under limited N supply (Fig. 3). Indeed, the slope of leaf area growth decreased from 16.4×10^{-4} m^2 °Cd^{-1} for the high-fertilized treatment 'd' (Fig. 3, Exp.3.1) to 1.2×10^{-4} m^2 °Cd^{-1} for the non-fertilized treatment 'a' (Fig. 3, Exp.1.2). The duration of plant leaf growth ranged from 1160 °Cd for 'd' (Fig. 3, Exp.3.1) to 936 °Cd for 'a' (Fig. 3, Exp.2.1). Ultimately, the maximum plant leaf area reached 1.68 m^2 for 'd' (Fig. 3, Exp.3.1), while it was 0.17 m^2 for 'a' (Fig. 3, Exp.1.2). The maximum plant leaf area observed in the high-fertilized treatment 'd' was much lower in Exp.1.1 (0.98 m^2) than in the other experiments, probably due to the lower N supply in this experiment (1.84 g) compared with the N supply in the other high-N treatments across all experiments (>4.10 g) (Table 1).

Interestingly, the organic fertilizer ('e') showed similar slopes (~6×10^{-4} m^2 °Cd^{-1} for Exp.1.1, Exp.1.2, and Exp.2.1, and 9.7×10^{-4} m^2 °Cd^{-1} for Exp.3.1) and maximum plant leaf area (~0.6 m^2 for Exp.1.1, Exp.1.2, Exp.2.1, and Exp.2.2, and 0.97 m^2 for Exp.3.1) to the mineral treatment with half the amount of N supply ('b'). Lastly, the results underlined a more important reduction in plant leaf area after 2 successive years of N starvation (Exp.1.1 versus Exp.1.2, treatment 'a'). Indeed, the maximum plant leaf area for treatment 'a' was lower in the second year (0.17 m^2) than in the first year (0.38 m^2), whereas for the high N supply treatment 'd', the maximum plant leaf area was higher in the second year (1.32 m^2) than in the first year (0.98 m^2).

The slope and duration of plant leaf area growth were expressed as a function of median SPAD index reading until flowering and C storage at budburst (Fig. 1A, Eq. 3). Both parameters increased significantly with SPAD index and decreased significantly with C storage (Table 4). A gain of 1 unit of SPAD index until flowering was associated with increases in the leaf growth slope of 1.86 cm^2 °Cd^{-1} and the duration of leaf growth of ~12.45 °Cd. In contrast, an increment of initial C storage of 1 g was concomitant with a decrease in both the slope of leaf growth, by 7.49 cm^2 °Cd^{-1}, and its duration, by 34.88 °Cd.

Quantification of the effect of SPAD index and leaf area on DM production

The increase of plant leaf area explained 88% of the observed DM produced per MJ of global radiation [CI=(1.44×10^{-2}, 9.14×10^{-2})]. On average, the DM produced increased by 0.05 g DM MJ^{-1} per square metre of additional leaf area. By contrast, the mean SPAD index readings from budburst to flowering did not significantly impact the biomass increment per MJ of global radiation [CI=(-22×10^{-4}, 35×10^{-4})] (Fig. 4).

Estimation of the effect of DM production on the allocation of DM to plant organs

The rules of allocation of DM towards the storage, perennials, leaves, shoots, and clusters, according to DM production per MJ of global radiation, depended on the phenological stages (Fig. 1C; Fig. 5). However, responses were globally more marked for annual organs, especially shoots and leaves, and less marked for perennial organs.

The storage decreased before flowering, and started to be restored thereafter (see Fig. 2G–I). The remobilization of carbohydrates from storage pre-flowering (B1→F1) reached 48% on average (Fig. 5A). The measured reallocation of carbohydrates to the storage pool ranged from 0% to 24% from flowering to veraison (F1→V1), from 0% to 41% from veraison to harvest (V1→H1), and from 18% to 51% after harvest (H1→B2). The restoration of storage significantly decreased when the total DM per MJ increased during the period from flowering to veraison (F1→V1): it was ~42% lower when DM production increased by 0.10 g DM MJ^{-1}.

Table 4. Posterior estimation of the effects of SPAD index (budburst to flowering) and initial storage (in g, at budburst) on the slope and duration of leaf area increase using a Bayesian framework (see Eq. 3 for further details) on the same experiment and N treatments as in Fig. 3

	Leaf area slope (b_i in Eq. 3, in cm² °Cd⁻¹)	Thermal time to reach maximum leaf area (TT_{LAmax_i} in Eq. 3, in °Cd)
SPAD index (B1→F1)	$b.slope.S$=1.86±0.27	$TT.slope.S$=12.47±4.65
	CI=(1.5, 2.3)	CI=(4.6, 19.6)
Storage (B1)	$b.slope.C$=–7.49±1.45	$TT.slope.C$=–34.88±3.72
	CI=(–10.3, –5.8)	CI=(–40.3, –29.7)
Intercept	μ_b=53.44±3.21	μ_{TT}=1335.35±20.49
	CI=(48.2, 58.3)	CI=(1304, 1364)

Values represent means ±SD. CI, 95% credible interval.

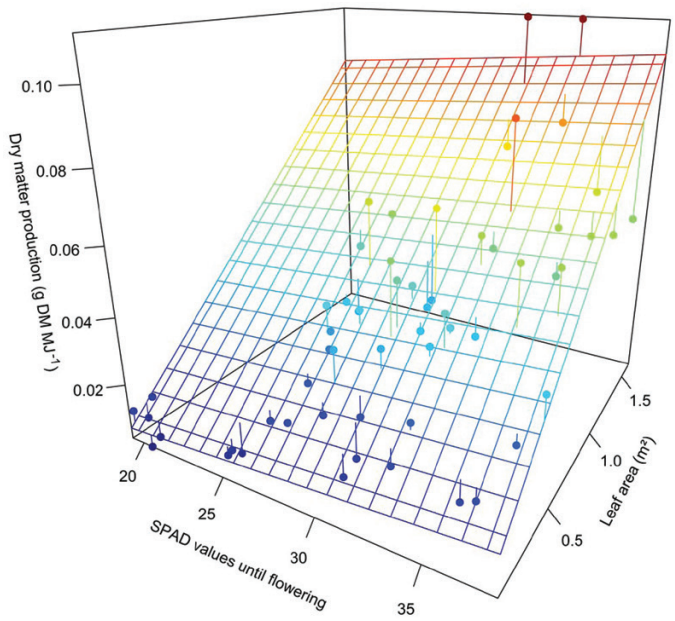

Fig. 4. DM production per unit of global radiation (g DM MJ^{-1}) according to mean SPAD index reading values until flowering and leaf area (m^2) at the same date as DM. Each point represents the mean value calculated for an experiment and an N treatment ('a', 'b', 'c', 'd' and 'e') at flowering, veraison (Exp.1.2, Exp.2.1, Exp.2.2, and Exp.3.1), and harvest (Exp.1.1, Exp.1.2, Exp.2.1, Exp.2.2, and Exp.3.1). The regression plane was obtained by a Bayesian approach (see Eq. 4 for further details); its equation is: DM production per unit of global radiation = -6.35×10^{-3} + 6.21×10^{-4} × SPAD + 5.29×10^{-2} × leaf area (mean estimate of R^2=0.88; see Supplementary Fig. S1 for further details).

The computed allocation of DM towards perennial organs (Fig. 5B) represented on average 4% from budburst to flowering (B1→F1), 32% from flowering to veraison (F1→V1), 20% from veraison to harvest (V1→H1), and 66% after harvest (H1→B2). No significant trend of DM production effect on the allocation towards the perennial pool was observed for any period.

The estimated intercept of DM allocation towards leaves (Fig. 5C) from budburst to flowering (B1→F1) was 61%. After flowering, the computed allocation to the leaves was lower, but it increased significantly when the plant DM production per MJ was higher. A gain of 0.10 g DM MJ^{-1} increased the allocation towards the leaves by ~32% from flowering to veraison (F1→V1), and by 10% from veraison to harvest (V1→H1).

Computed values of DM allocation towards the shoot (Fig. 5D) represented from 25% to 40% from budburst to flowering (B1→F1), from 10% to 30% from flowering to veraison (F1→V1), and from 13% to 22% from veraison to harvest (V1→H1). A gain of 0.10 g DM MJ^{-1} increased the allocation of shoot DM by 34% from budburst to flowering and by 20% from flowering to veraison.

Finally, the computed allocation of DM towards clusters (Fig. 5E) represented from 2% to 8% before flowering (B1→F1), from 17% to 24% from flowering to veraison (F1→V1), and from 21% to 39% until harvest (V1→H1). Although the allocation towards this pool was limited before flowering, a negative trend of DM production per MJ was observed at flowering (–99% of allocation to cluster per plant g DM MJ^{-1}).

Discussion

The Bayesian approach is necessary to consider uncertainty when dealing with destructive measurements and composite variables

The experimental design and the need to resort to destructive measurements to assess DM production, carbohydrate content, and leaf area implies the use of covariates with measurement error and composite variables. Moreover, studying the effect of N and C on latent variables such as the slope and duration of the leaf area growth dynamics led us to choose a Bayesian approach, which better considers all sources of variability and introduces expert knowledge (as a prior) to constraint estimation of parameters in a restricted range.

Using priors allows the estimations to converge

The use of a prior permits the analysis to proceed when the dataset is too small; as a result, the posterior estimation is a mixture between data and prior. In Eq. 2, we used two priors, without which no convergence in a plausible biological range would be possible due to the lack of data. First, we imposed that leaf area plateaued with a normal distribution centred at 1400 °Cd after budburst according to previous studies (Valdés-Gómez *et al.*, 2009; Zufferey *et al.*, 2012). Second, the starting point of the period of growth was fixed from our dataset and from our knowledge during the pre-flowering period (Munitz *et al.*, 2016) at 150 °Cd in abscise with a random ordinate distributed from a normal distribution centred at 300 cm^2.

Composite variables

The Bayesian model was able to simultaneously estimate all parameters in sub-models 1, 2, and 3. The simultaneous estimation is of great concern. Poor results (Supplementary Fig. S2) were obtained when we proceeded to independent estimation of sub-model 1 (Bayesian segmented regression to estimate leaf area slopes and thermal times), sub-model 2 (ANOVA for initial carbohydrate and SPAD index mean estimates) and then sub-model 3 (multiple linear regression to link leaf area dynamics to mean estimates of carbohydrate and SPAD index).

Uncertainties due to destructive measurements

The Bayesian integrated model provided a good prediction of leaf area and SPAD index until flowering, and a coherent estimation of carbohydrates at budburst. For the SPAD index readings, the estimates from the Bayesian integrated model were close to the measurements. In contrast, the estimated

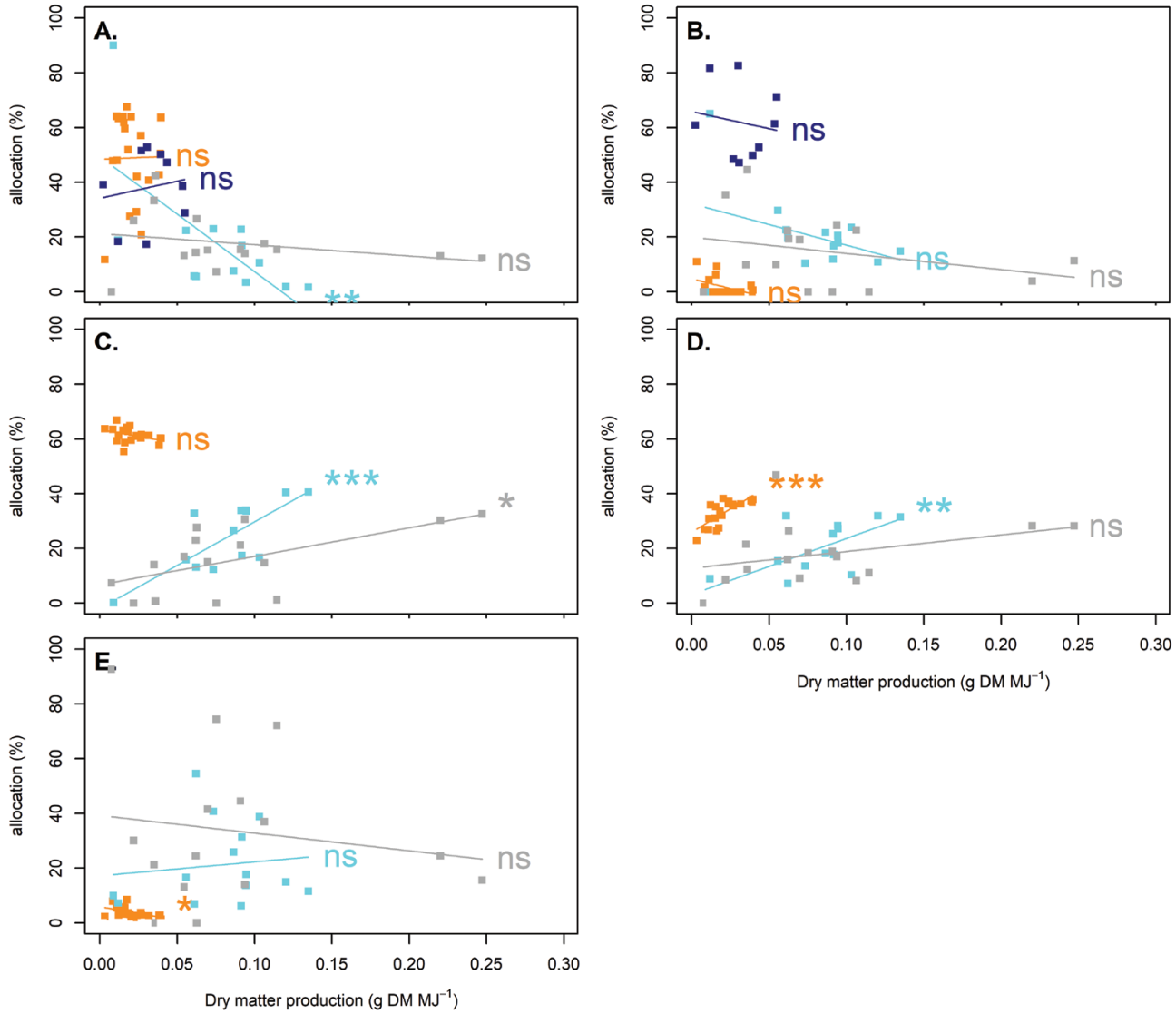

Fig. 5. Allocation coefficients towards storage (A), perennial (B), leaves (C), shoot (D), and clusters (E) as a function of DM production per unit of global radiation (g DM MJ^{-1}). The different colours represent the period (orange, B1→F1; light blue, F1→V1; grey, V1→H1; blue, H1→ B2). The lines give the linear trends between DM production and allocation coefficients. The trends were tested by *F*-tests for each period/organ and significant differences are indicated with asterisks (**P*<0.05, ***P*<0.01, ****P*<0.001; ns, non-significant).

values of mean carbohydrate at budburst were lower and less variable between treatments (4.22–8.48 g per plant) than carbohydrate sample mean values (1.98–38.21 g per plant). However, the ranking of treatment mean values across experiments was the same in both estimations. To explain this shrinkage, several hypotheses could be proposed. First, we sampled from three to five plants per treatment in a global population of 110–150 plants depending on the batch. Due to this small sample size, initial carbohydrate estimation might be sensitive to the prior, the consequence being that posterior marginal distribution might not be driven enough by the carbohydrate data but more by the prior on the leaf area dynamic. This shrinkage effect is well known and described in Bayesian modelling (as a distinction between Best Linear Unbiased Predictor and Best Linear Unbiased Estimator estimate values). Second, the usual sample mean value may be an incorrect estimation due to the complexity of correctly extracting and washing roots without any loss during hand-washing. Third, the difference between the two estimations (sampled mean versus Bayesian integrated estimation) could come from carbohydrate analysis: this is particularly the case with soluble sugars, for which high variability is observed during extraction and dosage (Quentin *et al.*, 2015). Regarding the two last points, the coefficients of variation for a given N treatment and date were 29% and 28% for biomass and soluble sugars, respectively.

A Bayesian approach was also used to quantify the DM production responses to N treatments (Fig. 4) and revealed that changes in leaf area were mainly responsible for the variation in DM. When a frequentist approach that does not integrate this variability was used, a significant effect of SPAD index on biomass production (Supplementary Table S1; P=0.02) shows a probably underestimated risk of error (type I).

N supply affects C balance over the cropping seasons

Lower mineral N fertilization decreased leaf area and plant C production

Leaf growth sharply increased from budburst to veraison and then progressively plateaued (Fig. 3). Moreover, low SPAD index until flowering and high carbohydrate reserves at budburst reduced the rate and duration of leaf area growth (Figs 1, 5). The positive role of N uptake on the laminae surface, the number of primary and secondary leaves, and the leaf/fruit ratio in grapevines has been clearly established (Metay *et al.*, 2014; Zufferey *et al.*, 2015). However, the negative effect of carbohydrate reserves at budburst on leaf area seems discordant with previous findings. Notably, Zufferey *et al.* (2012) and Goffinet (2004) stated that depleted starch reserves at budburst induced depressed shoot growth and leaf area per shoot. This difference could be explained by the distortion in the estimation of carbohydrate reserves at budburst (Supplementary Table S2).

The reduction of plant DM production from flowering to veraison was mainly due to the lower plant leaf area (Figs 1–3, Table 4), as shown in previous studies (Zerihun and Treeby, 2002). Although the plant leaf growth progressively plateaued from veraison, the differences in DM among treatments increased afterwards (Fig. 1). In contrast, the SPAD index had little effect on the plant DM production per unit of global radiation (Fig. 4). Prieto *et al.* (2012) reported that N content per leaf area was a good predictor of the variation of photosynthetic activity within the canopy. This raises the question of the representativeness of the SPAD index measured on one leaf in our study compared with the whole-canopy N status. In addition, the fact that we used SPAD index readings instead of N content per unit area could distort the relationship between N status and DM production due to the plateauing of SPAD values at high N content (Cerovic *et al.*, 2012). Our results also suggested that the effects of C and N were amplified in the second year of experimentation on the plant leaf area dynamics but did not impact the C production efficiency.

Ultimately, although the rootstock used in our study (SO4) is likely to have influenced the scion response to N, a lower effect of rootstock when compared with the effects of N or of the scion and only little interaction between N and the rootstock on the scion functioning have been reported (Keller *et al.*, 2001*a*, *b*; Zerihun and Treeby, 2002; Tandonnet *et al.*, 2008; Ibacache *et al.*, 2020).

Lower mineral N fertilization only poorly changed the coefficients of biomass allocation

In our study, C allocation depended more on phenological stages (which were little impacted by N treatments, see Supplementary Table S3) than on C availability (Fig. 5). Before flowering, C was mainly allocated towards the shoots and leaves, regardless of N supply, similar to the results of Nogueira Júnior *et al.*, (2018). Consequently, the higher DM of leaves observed in well-N-supplied treatments was due to higher C production rather than higher allocation towards this organ. Lower DM production decreased the C allocation towards the fruits before flowering, but had no effect on the allocation towards the fruits after flowering. By contrast, a negative effect of low N on both the initiation of inflorescence primordia in latent buds and on fruit set was reported by Keller (2010) and Guilpart *et al.*, (2014). Regarding the storage, we observed a similar pattern to that reported in other studies (Scholefield *et al.*, 1978; Conradie, 1980; Zapata *et al.*, 2004; Pradubsuk and Davenport, 2010), with a translocation of C from woody tissues to support the growth of emerging shoots before flowering.

Other factors may deserve more consideration to improve the consistency between measured and estimated DM in each organ. Some studies have suggested that C allocation is driven by, in addition to N, light and water availability (Ezzahouani *et al.*, 2007; Grechi *et al.*, 2007). The 3 years of the experiments showed contrasting weather conditions (Table 1). Notably, 2019 was characterized by a cold spring (–3.35 °C compared with 2017 and 2018) and an intense peak of heat 1 month after flowering (10 d with temperature >35°C) and a higher cumulated light (+640 MJ m^{-2} compared with 2017 and 2018), which caused thermal stress to the plants. In contrast, 2018 was rainy until veraison (305 mm) and 2017 was dry (67 mm). This between-year variability in weather probably impacted C allocation and yield development (Zhu *et al.*, 2020), but it could not be assessed in this work due to the complexity of considering each climatic factor separately. Additional studies under controlled conditions would be required to assess the specific role of temperature, water availability, or light intensity on C allocation (Torregrosa *et al.*, 2017; Luchaire *et al.*, 2017). Multi-local experiments to obtain contrasting climatic conditions may also be relevant in this regard (Zhu *et al.*, 2020; Laurent *et al.*, 2021).

Specific N supply management consequences

Our work dealt with two specific cases of N management: the absence of N fertilization, which is quite common in the case of low yield objectives, and organic fertilization, which is widespread in organic viticulture. When no N was supplied (treatment 'a'), we observed a very low leaf area (<0.4 m^2) and DM production (<107g) at harvest, in agreement with the study reported by Metay *et al.* (2014). Under conditions of C and N starvation, the main sink organs became the perennial organs

and, to a lesser extent, the fruit, as observed by other authors (Rodriguez-Lovelle and Gaudillère, 2002; Zerihun and Treeby, 2002). The effect of N starvation seemed to be limited when C reserves were higher: we observed similar leaf area dynamics and DM at harvest for treatment 'a' in Exp.3.1 (28.49 g DM) compared with the 'b' treatments in the other experiments (8.56–12.32 g DM). This reinforced the difficulty in properly anticipating the consequences of N stress in perennial plants due to the reserve pool (Conradie, 1991; Holzapfel *et al.*, 2010).

When organic fertilization was supplied (treatment 'e'), our results indicated a slower dynamics of leaf area and SPAD index readings compared with the mineral fertilization treatment containing the same amount of N (treatment 'c'). SPAD index (Table 1) and leaf area dynamics (Figs 2, 3) for the organic treatment were similar to the dynamics with the mineral treatment at half the dose of mineral N (treatment 'b'), suggesting that only 50 % of the N supply was released before veraison. This low N release could be explained by the substrate used (a mixture of blond and black sphagnum peat moss, peat fibre, and fine clay), which could limit the soil biological activity that is essential for the mineralization of organic fertilizer. This observation clearly underlines the need to consider the kinetics of N release when using organic fertilizers or green manure (Conradie, 2001; Ripoche *et al.*, 2011) and to adapt N management (particularly the timing of application) to avoid any risk of N deficiency during the most sensitive periods for production (i.e. flowering/veraison).

Non-destructive SPAD index measurement is useful to control N status

Non-destructive methods such as SPAD index measurement were developed to provide fast, cheap, and repeatable assessments of leaf N (Brunetto *et al.*, 2012). The use of SPAD index values in the present study allowed us to (i) identify the contrasting kinetics of N availability to the plant between organic and mineral fertilizers (Brunetto *et al.*, 2012; Cerovic *et al.*, 2015; Vrignon-Brenas *et al.*, 2019) and (ii) adjust the N supply in real-time through fertilization management (Van Leeuwen *et al.*, 2000).

In spite of the advantages of the non-destructive methods described above, they generally require calibration. For instance, the relationship between SPAD index and leaf N content is cultivar-specific (Brunetto *et al.*, 2012), non-linear for suboptimal N contents (Cerovic *et al.*, 2012), and dependent on specific leaf area (Cerovic *et al.*, 2015). In addition, the SPAD index measured on one leaf may not be representative of the overall plant leaf N status. However, the use of non-destructive methods, once they have been calibrated, generally provides a time saving compared with hand-harvested measurements (e.g. SPAD index versus assay of leaf N). In addition, experimental designs using non-destructive measurements permit measurement of the different variables on the same individuals, therefore avoiding the risk of an 'in and out of sample' error and the need to use specific statistical methods.

Perspectives: towards a model integrating the effect of N supply at the pluriannual scale

The complexity of the processes involved in pluriannual grapevine growth requires an integrative approach to grapevine N nutrition management (Verdenal *et al.*, 2021). In this study, we proposed a global conceptual framework of C balance in grapevines based on the assumption that C production per unit of incident global radiation is driven by the leaf area, this latter depending on SPAD and reserves. This representation of DM production is consistent with most crop models (Bindi *et al.*, 1997; Nendel and Kersebaum, 2004; Lakso and Poni, 2005; Garcia de Cortazar-Atauri, 2006; Nogueira Júnior *et al.*, 2018). However, only few of the above models simulate the pluriannual effect of N supply on C balance. In their model, Nogueira Júnior *et al.* (2018) integrated the effect of N on the reallocation from trunk and roots (i.e. 'perennial' organs in our study) to take into account the role of reserves at the pluriannual scale. Our study brings new knowledge to quantify the effect of N constraints on leaf area dynamics, C production, and its allocation towards organs depending on phenological stages over several cropping seasons, taking into account carbohydrate reserves at budburst. The Bayesian approach also underlined that care must be taken about uncertainty in carbohydrate measurements, in particular concerning initializing storage. This point is crucial, as DM increments before flowering rely on the pool of reserves stored during the previous year (Yang and Hori, 1980; Bates *et al.*, 2002; Zapata *et al.*, 2004).

From a modelling perspective, further research is needed to replace SPAD index readings by, first, the dynamics of leaf N content and, second, the dynamics of plant N uptake and N remobilization. However, SPAD index readings, which allow an easy assessment of the N status, may be useful to calibrate a model of soil N balance, such as the existing soil models DAISY (Hansen *et al.*, 2012), EPIC (Izaurralde *et al.*, 2006), or the model proposed by Nendel and Kersebaum (2004) for vineyard soils. It will also be essential to simulate the seasonal fluxes of N to and from the storage compartment, in addition to carbohydrates (Schreiner, 2016).

Lastly, in our experimental conditions using pots, the grapevines were well watered so that the water regime could not be considered as a stress or limiting factor. However, in an on-farm modelling approach, water deficit should also be considered both for the link with soil N balance models and to reflect real conditions in vineyards.

Conclusion

Our study brought new insights to modelling at the whole-plant scale the seasonal effect of various N constraints on grapevine leaf area, DM production, and allocation towards vegetative and reproductive organs. We also reinforced our understanding of the pluriannual effect of N nutrition on grapevine growth by taking into account non-structural carbohydrates in perennial

organs. The effects of N status and initial carbohydrate reserves on leaf area dynamics, quantified using a Bayesian approach, revealed a distortion between estimated and measured carbohydrate content. The counterintuitive negative impact of reserves on leaf area should thus be considered with caution. Based on the Bayesian approach, the DM production under N supply mainly relied on plant leaf area. Lastly, our study showed that the allocation of C towards plant vegetative organs (leaves and shoots) after flowering increased when the rate of plant C production was higher, at the expense of storage reallocation. In contrast, the allocation of C towards the perennial organs (roots and trunk) and fruits was weakly influenced by the rate of plant C production. Consequently, the final yield and reserves mainly depended on plant leaf area growth rate and duration.

We considered in our Bayesian approach the potential effect of the 'in and out of sample' error due to the destructive measurements of variables such as biomass or carbohydrates. This method was shown to improve the agreement between measured and simulated leaf area dynamics thanks to the use of priors (expert knowledge) and the hierarchical structure. These results, linked to the conceptual framework proposed in our study, could be used in a future modelling perspective to simulate the pluriannual growth of grapevines under various N supply conditions using a limited set of parameters.

Supplementary data

The following supplementary data are available at *JXB* online.

Fig. S1. Posterior distributions of the R^2 and the leaf area parameter.

Fig. S2. Time course of leaf area as a function of cumulated thermal time after budburst, according to the experiments and N treatments.

Table S1. Result of the frequentist approach to explore the effects of SPAD index and leaf area at the same date as DM measurement on the DM production per unit of global radiation.

Table S2. Some more results for the leaf area model.

Table S3. Duration of the different periods between the main phenological stages, according to the experiments and N treatments.

Acknowledgements

The authors would like to thank Aurélien Ausset for his technical support and the partners of the project, notably from ITK, Frayssinet, Lallemand, and Nyseos.

Author contributions

SVB, AP, AM, BF, JC, and DF: conceptualization; SVB, BF, AB, and JC: data curation; SVB, BF, and GR: formal analysis; AP, AM, BF, and DF: funding acquisition; AP and AM: investigation; AP, AM, and BF: methodology; AP, AM, BF, and DF: project administration; AP, AM, and BF: supervision; SVB and BF: visualization; SVB, AP, AM, and BF: writing—original draft; JC, DF, SVB, AP, AM, and BF: writing—review and editing.

Conflict of interest

The authors declare no conflict of interest.

Funding

This study was supported by the Fond Unique Interministériel (FUI n°21) as part of the project NV2.

Data availability

The data supporting the findings of this study are available from the corresponding author, Anne Pellegrino, upon request.

References

Abay KA, Abate GT, Barrett CB, Bernard T. 2019. Correlated non-classical measurement errors, 'Second best' policy inference, and the inverse size-productivity relationship in agriculture. Journal of Development Economics **139**, 171–184.

Arima S, Datta GS, Liseo B. 2012. Objective Bayesian analysis of a measurement error small area model. Bayesian Analysis **7**, 363–384, 322.

Bates TR, Dunst RM, Joy P. 2002. Seasonal dry matter, starch, and nutrient distribution in 'Concord' grapevine roots. American Society for Horticultural Science **37**, 313–316.

Benjamini Y, Hochberg Y. 1995. Controlling the false discovery rate: a practical and powerful approach to multiple testing. Journal of the Royal Statistical Society: Series B (Methodological) **57**, 289–300.

Bindi M, Miglietta F, Gozzini B, Orlandini S, Seghi L. 1997. A simple model for simulation of growth and development in grapevine (*Vitis vinifera* L.). II. Model validation. Vitis **36**, 73–76.

Brunetto G, Melo GW, Toselli M, Quartieri M, Tagliavini M. 2015. The role of mineral nutrition on yields and fruit quality in grapevine, pear and apple. Revista Brasileira de Fruticultura **37**, 1089–1104.

Brunetto G, Trentin G, Ceretta CA, Girotto E, Lorensini F, Miotto A, Zaferi Moser GR, Wellington de Melo G. 2012. Use of the SPAD-502 in estimating nitrogen content in leaves and grape yield in grapevines in soils with different texture. American Journal of Plant Sciences **3**, 1546–1561.

Cerovic ZG, Ghozlen NB, Milhade C, Obert M, Debuisson S, Le Moigne M. 2015. Nondestructive diagnostic test for nitrogen nutrition of grapevine (*Vitis vinifera* L.) based on dualex leaf-clip measurements in the field. Journal of Agricultural and Food Chemistry **63**, 3669–3680.

Cerovic ZG, Masdoumier G, Ghozlen NB, Latouche G. 2012. A new optical leaf-clip meter for simultaneous non-destructive assessment of leaf chlorophyll and epidermal flavonoids. Physiologia Plantarum **146**, 251–260.

Che X, Xu S. 2010. Bayesian data analysis for agricultural experiments Canadian Journal of Plant Science **90**, 575–602.

Chesher A. 1991. The effect of measurement error. Biometrika **78**, 451–462.

Conradie WJ. 1980. Seasonal uptake of nutrients by Chenin blanc in sand culture: I. Nitrogen. South African Journal for Enology and Viticulture. **1**, 59–65.

Conradie WJ. 1991. Distribution and translocation of nitrogen absorbed during early summer by two-year-old grapevines grown in sand culture. American Journal of Enology and Viticulture **42**, 180.

Conradie W. 2001. Timing of nitrogen fertilisation and the effect of poultry manure on the performance of grapevines on sandy soil. I. Soil analysis, grape yield and vegetative growth. South African Journal of Enology and Viticulture **22**, 53–59.

Draper NR, Smith H. 1998. Applied regression analysis, 3rd Ed. Hoboken: John Wiley & Sons.

Ekbic H, Ozdemir G, Sabir A, Tangolar S. 2010. The effects of different nitrogen doses on yield, quality and leaf nitrogen content of some early grape cultivars (*V. vinifera* L.) grown in greenhouse. African Journal of Biotechnology **9**, 5108–5112.

Evans JR. 1989. Photosynthesis and nitrogen relationships in leaves of C_3 plants. Oecologia **78**, 9–19.

Ezzahouani A, Valancogne C, Pieri P, Amalak T, Gaudillère J-P. 2007. Water economy by Italia grapevines under different irrigation treatments in a Mediterranean climate. OENO One **41**, 131–139.

Garcia de Cortazar-Atauri I. 2006. Adaptation du modèle STICS à la vigne (Vitis vinifera L.): utilisation dans le cadre d'une étude d'impact du changement climatique à l'Échelle de la France. PhD Thesis, École National Supérieure Agronomique de Montpellier.

Gelman A, Carlin JB, Stern HS, Rubin DB. 2004. Bayesian data analysis. 2nd Ed. Boca Raton: Chapman & Hall/CRC.

Goffinet MC. 2004. Anatomy of grapevine winter injury and recovery. Departmental research paper. Geneva: Department of Horticultural Services, Cornell University.

Gomez L, Rubio E, Lescourret F. 2003. Critical study of a procedure for the assay of starch in ligneous plants. Journal of the Science of Food and Agriculture **83**, 1114–1123.

Grechi I, Vivin P, Hilbert G, Milin S, Robert T, Gaudillère JP. 2007. Effect of light and nitrogen supply on internal C:N balance and control of root-to-shoot biomass allocation in grapevine. Environmental and Experimental Botany **59**, 139–149.

Guilpart N, Metay A, Gary C. 2014. Grapevine bud fertility and number of berries per bunch are determined by water and nitrogen stress around flowering in the previous year. European Journal of Agronomy **54**, 9–20.

Hansen S, Abrahamsen P, Petersen C, Styczen M. 2012. Daisy: model use, calibration, and validation. American Society of Agricultural and Biological Engineers **55**, 1317–1333.

Holzapfel BP, Smith JP, Field SK, Hardie WJ. 2010. Dynamics of carbohydrate reserves in cultivated grapevines. Horticultural Reviews **37**, 143–211.

Ibacache A, Verdugo-Vásquez N, Zurita-Silva A. 2020. Rootstock:scion combinations and nutrient uptake in grapevines. In: Srivastava AK, Hu C, eds. Fruit crops. Amsterdam: Elsevier, 297–316.

Izaurralde RC, Williams JR, McGill WB, Rosenberg NJ, Jakas MCQ. 2006. Simulating soil C dynamics with EPIC: model description and testing against long-term data. Ecological Modelling **192**, 362–384.

Jensen SM, Svensgaard J, Ritz C. 2020. Estimation of the harvest index and the relative water content – two examples of composite variables in agronomy. European Journal of Agronomy **112**, 125962.

Keller M. 2010. Managing grapevines to optimise fruit development in a challenging environment: a climate change primer for viticulturists. Australian Journal of Grape and Wine Research **16**, 56–69.

Keller M, Kummer M, Vasconcelos MC. 2001a. Reproductive growth of grapevines in response to nitrogen supply and rootstock. Australian Journal of Grape and Wine Research **7**, 12–18.

Keller M, Kummer M, Vasconcelos MC. 2001b. Soil nitrogen utilisation for growth and gas exchange by grapevines in response to nitrogen supply and rootstock. Australian Journal of Grape and Wine Research **7**, 2–11.

Kvålseth TO. 1985. Cautionary note about R^2. The American Statistician **39**, 279–285.

Lakso AN, Poni S. 2005. "Vitisim" – a simplified carbon balance model of a grapevine. XIV International GESCO Viticulture Congress. Geisenheim: Groupe d'Etude des Systemes de Conduite de la Vigne (GESCO), 478–484.

Laurent C, Oger B, Taylor JA, Scholasch T, Metay A, Tisseyre B. 2021. A review of the issues, methods and perspectives for yield estimation, prediction and forecasting in viticulture. European Journal of Agronomy **130**, 126339.

Loescher WH, McCamant T, D. KJ. 1990. Carbohydrate reserves, translocation, and storage in woody plant roots. American Society for Horticultural Science **25**, 274–281.

Luchaire N, Rienth M, Romieu C, Nehe A, Chatbanyong R, Houel C, Ageorges A, Gibon Y, Turc O, Muller B, Torregrosa L, Pellegrino A. 2017. Microvine: a new model to study grapevine growth and developmental patterns and their responses to elevated temperature. American Journal of Enology and Viticulture, ajev.**2017**.16066.

Lunn D, Spiegelhalter D, Thomas A, Best N. 2009. The BUGS project: evolution, critique and future directions. Statistics in Medicine **28**, 3049–3067.

Marin JM, Robert CP. 2007. Bayesian Core: a practical approach to computational Bayesian statistics. New York: Springer.

Metay A, Magnier J, Guilpart N, Christophe A. 2014. Nitrogen supply controls vegetative growth, biomass and nitrogen allocation for grapevine (cv. Shiraz) grown in pots. Functional Plant Biology **42**, 105–114.

Monteith JL, Moss CJ, Cooke GW, Pirie NW, Bell GDH. 1977. Climate and the efficiency of crop production in Britain. Philosophical Transactions of the Royal Society of London. B, Biological Sciences **281**, 277–294.

Mooney H, Gartner BL. 1991. Reserve economy of vines. In Putz FE, Mooney HA, eds. The biology of vines. Cambridge: Cambridge University Press, 161–179.

Muff S, Riebler A, Held L, Rue H, xe, vard, Saner P. 2015. Bayesian analysis of measurement error models using integrated nested Laplace approximations. Journal of the Royal Statistical Society. Series C (Applied Statistics) **64**, 231–252.

Munitz S, Schwartz A, Netzer Y. 2016. Evaluation of seasonal water use and crop coefficients for Cabernet Sauvignon grapevines as the base for skilled regulated deficit irrigation. Leuven: International Society for Horticultural Science, 33–40.

Nendel C, Kersebaum KC. 2004. A simple model approach to simulate nitrogen dynamics in vineyard soils. Ecological Modelling **177**, 1–15.

Nogueira Júnior AF, Amorim L, Savary S, Willocquet L. 2018. Modelling the dynamics of grapevine growth over years. Ecological Modelling **369**, 77–87.

Pollice A, Jona Lasinio G, Rossi R, Amato M, Kneib T, Lang S. 2019. Bayesian measurement error correction in structured additive distributional regression with an application to the analysis of sensor data on soil–plant variability. Stochastic Environmental Research and Risk Assessment **33**, 747–763.

Pradubsuk S, Davenport JR. 2010. Seasonal uptake and partitioning of macronutrients in mature 'Concord' grape. Journal of the American Society for Horticultural Science **135**, 474.

Prieto JA, Louarn G, Perez Peña J, Ojeda H, Simonneau T, Lebon E. 2012. A leaf gas exchange model that accounts for intra-canopy variability by considering leaf nitrogen content and local acclimation to radiation in grapevine (*Vitis vinifera* L.). Plant, Cell & Environment **35**, 1313–1328.

Quentin AG, Pinkard EA, Ryan MG, *et al.* 2015. Non-structural carbohydrates in woody plants compared among laboratories. Tree Physiology **35**, 1146–1165.

R Core Team. 2019. R: a language and environment for statistical computing. Vienna, Austria: R Foundation for Statistical Computing. http://www.R-project.org/

Ripoche A, Metay A, Celette F, Gary C. 2011. Changing the soil surface management in vineyards: immediate and delayed effects on the growth and yield of grapevine. Plant and Soil **339**, 259–271.

Rodriguez-Lovelle B, Gaudillère J-P. 2002. Carbon and nitrogen partitioning in either fruiting or non-fruiting grapevines: effects of nitrogen limitation before and after veraison. Australian Journal of Grape and Wine Research **8**, 86–94.

Rolland G. 2020. Choix d'une méthode d'extraction et de purification pour le dosage des sucres solubles et de l'amidon dans les tissus ligneux de la vigne. Le Cahier des Techniques INRAE **100**, Art3.

Rossouw GC. 2017. Grapevine carbohydrate and nitrogen allocation during berry maturation: Implications of source-sink relations and water supply. Doctoral Thesis, Charles Sturt University.

Scholefield PB, Neales TF, May P. 1978. Carbon balance of the sultana vine (*Vitis vinifera* L.) and the effects of autumn defoliation by harvest-pruning. Functional Plant Biology **5**, 561–570.

Schreiner RP. 2016. Nutrient uptake and distribution in young Pinot noir grapevines over two seasons. American Journal of Enology and Viticulture **67**, 436.

Tandonnet J-P, Soyer J-P, Gaudillère J-P, Decroocq S, Bordenave L, Ollat N. 2008. Long term effects of nitrogen and water supply on confered vigour and yield by SO4 and Riparia gloire de Montpellier rootstocks. OENO One **42**, 89–98.

Torregrosa L, Bigard A, Doligez A, *et al*. 2017. Developmental, molecular and genetic studies on grapevine response to temperature open breeding strategies for adaptation to warming. OENO One **51**, 155–165.

Valdés-Gómez H, Celette F, García de Cortázar-Atauri I, Jara-Rojas F, Ortega-Farías S, Gary C. 2009. Modelling soil water content and grapevine growth and development with the STICS crop-soil model under two different water management strategies. OENO One **43**, 13–28.

Van Leeuwen C, Friant P, Soyer J, Molot C, Chone X, Dubourdieu D. 2000. L'intérêt du dosage de l'azote total et de l'azote assimilable dans le moût comme indicateur de la nutrition azotée de la vigne. Journal International des Sciences de la Vigne et du Vin **34**, 75–82.

Verdenal T, Dienes-Nagy Á, Spangenberg JE, Zufferey V, Spring J-L, Viret O, Marin-Carbonne J, van Leeuwen C. 2021. Understanding and managing nitrogen nutrition in grapevine: a review. OENO One **55**, 1–43.

Vrignon-Brenas S, Metay A, Leporatti R, Gharibi S, Fraga A, Dauzat M, Rolland G, Pellegrino A. 2019. Gradual responses of grapevine yield components and carbon status to nitrogen supply. OENO One **53**, 289–306.

Yang Y, Hori Y. 1980. Studies on retranslocation of accumulated assimilates in 'Delaware' grapevines. III. Early growth of new shoots as dependent on accumulated and current year assimilates. Journal of Agricultural Research **31**, 120–129.

Zapata C, Deléens E, Chaillou S, Magné C. 2004. Partitioning and mobilization of starch and N reserves in grapevine (*Vitis vinifera* L.). Journal of Plant Physiology **161**, 1031–1040.

Zerihun A, Treeby MT. 2002. Biomass distribution and nitrate assimilation in response to N supply for *Vitis vinifera* L. cv. Cabernet Sauvignon on five *Vitis* rootstock genotypes. Australian Journal of Grape and Wine Research **8**, 157–162.

Zhu J, Fraysse R, Trought M, Raw V, Yang L, Greven M, Martin D, Agnew R. 2020. Quantifying the seasonal variations in grapevine yield components based on pre- and post-flowering weather conditions. OENO One **54**, 213–230.

Zufferey V, Murisier F, Belcher S, Lorenzini F, Vivin P, Spring JL, Viret O. 2015. Nitrogen and carbohydrate reserves in the grapevine (*Vitis vinifera* L. 'Chasselas'): the influence of the leaf to fruit ratio. Vitis **54**, 183–188.

Zufferey V, Murisier F, Vivin P, Belcher S, Lorenzini F, Spring J-L, Viret O. 2012. Carbohydrate reserves in grapevine (*Vitis vinifera* L.'Chasselas'): the influence of the leaf to fruit ratio. Vitis **51**, 103–110.